Research on Chemical Intermediates (2022) 48:4553–4577
https://doi.org/10.1007/s11164-022-04818-2

Magnetic starch as green supports for cobalt nanoparticles: efficient, eco-friendly, and economical catalyst for Mizoroki–Heck and Suzuki–Miyaura reactions

Nadiya Koukabi[1] · **Maryam Arghan**[1]

Received: 26 May 2022 / Accepted: 12 August 2022 / Published online: 5 September 2022

Abstract

In recent decades, the design of catalysts with features such as being readily recoverable from the reaction mixture, cost-effectiveness, efficiency, eco-friendly, and non-toxic is critical. Therefore, in this study, magnetic starch from apple seeds is suggested as a perfect substrate material with unique properties satisfying our need to minimize undesirable impacts on the environment. The magnetic starch acts as green support for cobalt nanoparticles to prepare Fe_3O_4@starch-Co(II) as an efficient heterogeneous catalyst in Mizoroki–Heck and Suzuki–Miyaura reactions. The fabricated catalyst was identified with several analysis techniques such as FT-IR, XRD, EDS, BET, TGA, FE-SEM, TEM, AAS, and elemental mapping. The catalyst performance reveals that it can be used as a promising replacement for palladium-based catalysts in the Mizoroki–Heck and Suzuki–Miyaura reactions. Because of the toxic nature of Pd-based materials, this catalyst can reduce the danger of using these catalysts. Also, due to the magnetic properties of the fabricated catalyst, the catalyst quickly separated from the reaction medium, and it is reusable for five runs without significant change in catalytic activity.

✉ Nadiya Koukabi
n.koukabi@semnan.ac.ir

[1] Department of Chemistry, Semnan University, Semnan 35131-19111, Iran

Graphical abstract

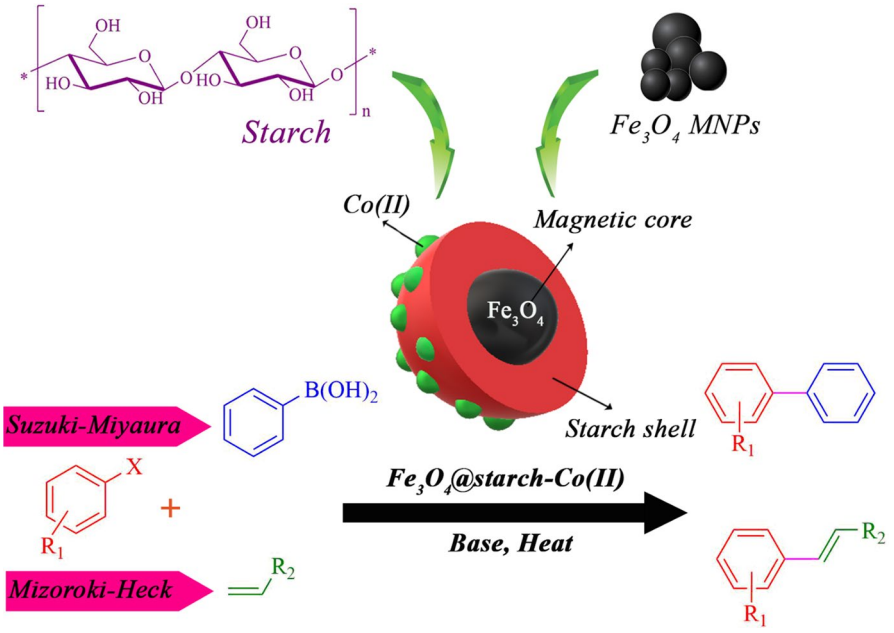

Keywords Starch · Magnetic catalyst · Mizoroki–Heck reaction · Suzuki–Miyaura reaction

Abbreviations

AAS	Atomic absorbtion spectroscopy
BET	Brunauer–Emmett–Teller analysis
BJH	Barrett–Joyner–Halenda analysis
EDS	Energy-dispersive spectroscopy
FT-IR	Fourier-transform infrared spectroscopy
FE-SEM	Field emission-scanning electron microscope
GC	Gas chromatography
TEM	Transmission electron microscopy
TGA	Thermogravimetric analysis
XRD	X-ray diffraction analysis
MCRs	Multi-component reactions
TLC	Thin-layer chromatography

Introduction

There is growing concern over environmental problems because of recent human activities; for this reason, following the principles of green chemistry in all research fields, particularly the synthesis of organic compounds, is important [1–3]. Scientists are always searching for processes and materials to achieve this ultimate goal. They are considering new ways to reduce the release of waste and hazardous substances into the environment [4–6]. For instance, in synthetic organic chemistry, methods and routes for the synthesis of green and biodegradable catalysts have received much attention, such as performing syntheses through one-pot multicomponent reactions (MCRs) instead of the traditional multi-step procedure [7–9]. One fashionable way to reach this goal is to use biocompatible and biodegradable materials. Natural macromolecular biopolymers are great candidates for developing new catalyst supports because of their unbeatable attributes, including chemical stability and being more eco-friendly than other commercial materials [10].

As polysaccharides are the most abundant biopolymers, it would be wise to replace them with synthetic polymers [5, 11, 12]. In addition, using waste materials is highly recommended and consistent with the green chemistry principles [13], so utilizing natural polysaccharides waste in catalyst making is an unprecedented step [14, 15]. In this regard, the preferable properties that catalyst supports should have are (a) environmentally friendliness, (b) high chemical and thermal stability, (c) low preparation cost, and (d) ease of chemical modification. Therefore, starch derived from apple seeds can be considered a great choice because of biodegradability, and above all, seeds come from waste [16]. So far, there are limited reports on apple seed starch application in various fields, especially catalysts [1, 16–18].

Apple seeds are rich in A-type starch [1, 19], and within the polysaccharide networks, amylum is the most considerable non-toxic, biodegradable, and biocompatible biopolymer [16, 20]. Because of abundant hydroxyl groups in polysaccharide structure, the apple seed starch can be directly utilized for the metal ions immobilization through ligand coordination or easily modified by oxidation, hydrolysis, esterification, or etherification [16, 21, 22].

Hence, starch-functionalized nanoparticles can be viewed as one of the best suitable catalysts for this aim. Among the various types of nanoparticles, Fe_3O_4 nanoparticles as magnetic nanoparticles have been involved in the fabrication of various heterogeneous catalysts to synthesize many organic compounds [1, 23]. These nanoparticles are inexpensive, non-toxic, and biocompatible, and their formation process is straightforward. One of the most significant disadvantages of these nanoparticles is the inherent instability that causes agglomeration and adverse effects on efficiency [23]. Therefore, functionalization of Fe_3O_4 significantly improves stability, whereby it increases surface area access and catalytically active sites.

In organic synthesis, Suzuki–Miyaura and Heck–Mizoroki C–C cross-coupling reactions are among the most fundamental reactions in organic synthesis due to

various applications in the synthesis of various drugs, and natural compounds, and organic building blocks [24–27]. Typically, for activating aryl halides to initiate the Heck–Mizoroki [28, 29] and the Suzuki–Miyaura [30–34] cross-coupling reactions, palladium catalysts are employed. Palladium as a catalyst for both reactions is highly active and uncompetitive, but it suffers from significant disadvantages, including air sensitivity, high cost, and toxicity of palladium complexes [35–37]. Thus, recent studies are concentrated on finding palladium alternatives resulting in replacing it with affordable transition metal catalysts such as iron, nickel, copper, and cobalt. The cobalt catalyst is a wise choice among the suggested alternatives because of its low cost, good activity, non-toxicity, and chemical stability. Thus, cobalt-based catalyst systems are well developed for both the Heck–Mizoroki and the Suzuki–Miyaura cross-coupling reactions.

In this study, we synthesized a magnetic catalyst that consists of a Fe_3O_4@starch component with a core–shell structure and cobalt ions immobilized on that. The starch shell, because of the abundant hydroxyl groups in its structure, plays two important roles; (1) Preventing the agglomeration and oxidation of Fe_3O_4 magnetic nanoparticles (MNPs) and (2) Providing a suitable substrate for the anchoring of formed cobalt ions. Also, due to its magnetic property, the iron core makes it easy to separate the catalyst from the reaction medium, and cobalt ions as active sites catalyze the Mizoroki–Heck and Suzuki–Miyaura coupling reactions.

Considering all the above-mentioned preferences, this report continues our previous effort to develop eco-friendly magnetically separable heterogeneous catalysts. This report reveals the successful synthesis of a cobalt-based magnetic catalyst via the incorporation of apple seed starch, Fe_3O_4 nanoparticles, and cobalt nanoparticles with a core–shell structure.

According to our knowledge, the catalytic activity of Fe_3O_4@starch-Co(II) in the Suzuki–Miyaura and Heck–Mizoroki reactions has not been reported to date. This catalyst was fabricated based on the green chemistry principle, and the separation of this heterogeneous catalyst is easily accomplished by placing a magnet at the end of the reaction vessel. Reusability for four runs and excellent yields in the Suzuki–Miyaura and Heck–Mizoroki reactions are other advantages of this catalyst.

Experimental

Chemicals and instruments

All the chemicals (reagents and solvents) were purchased from Merck and Sigma-Aldrich and were employed without further purification. The FT-IR spectra were recorded on a Shimadzu 8400S spectrometer using KBr pressed powder disks. XRD analysis was performed on a Siemens D5000 (Siemens AG, Munich, Germany) using Cu-Ka radiation of wavelength 1.54 Å. FE-SEM and EDS analyses were performed using TESCAN MIRA II digital scanning microscope. Also, TEM and BET analyses were performed by Philips EM 208S and Belsorp Mini II. TGA analysis was accomplished using a Du Pont 2000 thermal analysis apparatus heated from 25 to 1000 °C at a 5 °C/min heating rate under an air

atmosphere. The amount of cobalt in the catalyst was evaluated using an Agilent model 240 AA Shimadzu (USA) flame atomic absorption spectrometer. All measurements were carried out in an air/acetylene flame, and the Co hollow cathode lamps were used as the radiation sources. Thin-layer chromatography (TLC) on commercial plates coated with silica gel 60 F254 was applied to determine the purity of the products and the progress of the reactions. The NMR spectra were provided on Bruker Avance 400 MHz instruments (^{1}H-NMR 400 MHz and ^{13}C-NMR 125 MHz) in pure dimethyl sulfoxide. Detection of the products was performed by a gas chromatograph (GC-17A, Shimadzu, Japan) equipped with a splitless/split injector and a flame ionization detector. Helium (purity 99.999%) was used as the carrier gas at the constant flow rate of 4 mL min^{-1}. The temperatures of the injector and detector were set at 275 °C and 320 °C, respectively. The injection port was operated at splitless mode and with a sampling time of 1 min. For FID, hydrogen gas was generated with a hydrogen generator (OPGU-2200S, Shimadzu, Japan). A 30 m BP-10 SGE fused silica capillary column (0.32 mm i.d. and 0.25 μm film thickness) was applied for the separation of PAHs. The oven temperature program started from 60 °C, held for 3 min, increased to 190 °C at 20 °C min^{-1}, held for 0 min, increased to 240 °C at 10 °C min^{-1}, and then held for 3 min. A 10.0 μL ITO (Fuji, Japan) micro-syringe was applied for the collection of sedimented organic solvent and injection into the GC (GC-FID chromatograms 1,1′-biphenyl are shown in Figures 1S and 2S).

Preparation of Fe_3O_4 MNPs

Fe_3O_4 nanoparticles were prepared based on a procedure by Kolvari et al. 3 mL of $FeCl_3{\cdot}6H_2O$ in HCl was mixed with 10.33 mL of deionized water. In the next step, 2 mL of Na_2SO_3 (1 M) was also mixed with the previous solution under stirring. Afterward, the SO_3^{2-} and Fe^{3+} ions form a complex changing the mixture color from light yellow to red. To this solution, 80 mL of ammonia solution (0.85 M) was added under vigorous stirring. Upon the addition of the ammonia solution, the formation of a black precipitate occurs. The black precipitate crystallized after 30 min under stirring. The obtained Fe_3O_4 nanoparticles were collected by a magnet, followed by decanting and washing with deionized water. The Fe_3O_4 nanoparticles were dried in a vacuum oven at 65 °C for 12 h.

Preparation of starch from apple seeds

Apples were purchased from a local grocery. The apples were cut into pieces, and the seeds were removed from the apple slices with a knife. The separated seeds were crushed and pulverized into powder form. The seeds were peeled, and then, the residue was washed three times with ethyl acetate and two times with acetone to remove lipid and water. The powder was dried in a vacuum desiccator at 4 °C.

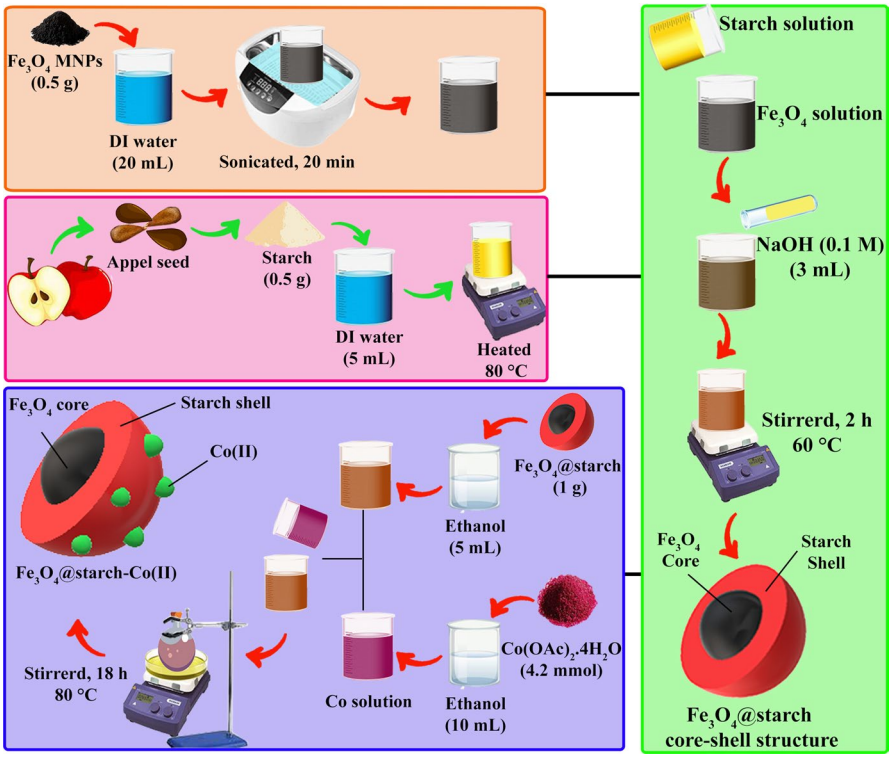

Scheme 1 The fabrication process of Fe_3O_4@starch-Co(II)

Preparation of Fe_3O_4@starch

Fe_3O_4 nanoparticles (0.5 g) were dispersed and sonicated in 20 mL of water for 20 min. 0.5 g of powder of apple seed starch was dissolved in 5 mL of water and heated to 80 °C. Afterward, it was added to the uniform solution of Fe_3O_4 nanoparticles. 3 mL of NaOH solution (0.1 M) was added dropwise to the previous mixture, followed by stirring for 2 hours at 60 °C. Finally, the catalyst particles were isolated by an external magnet and washed with ethanol and water, followed by drying at 50 °C.

Preparation of magnetic Fe_3O_4@starch-Co(II)

To anchor the Co nanoparticles on Fe_3O_4@starch as support, 4.2 mmol of $Co(OAc)_2{\cdot}4H_2O$ was dissolved in 10 mL of ethanol, followed by adding this solution to a uniform mixture of Fe_3O_4@starch in ethanol (1g Fe_3O_4@starch in 5 L ethanol). The mixture was kept under stirring for 18 h at 60 °C. Finally, the products were separated using a magnet and washed with ethanol, followed by drying at room temperature. The process of producing the catalyst is summarized in Scheme 1.

General procedure for the Mizoroki–Heck reaction

In a round-bottom flask with a magnetic stirrer, 1.5 mmol of olefin, 1 mmol of aryl halide, 4.0 mmol of K_3PO_4, Fe_3O_4@starch-Co(II) (0.4 mol%), and a mixture of H_2O (1.5 mL) and DMF (1.5 mL) were charged into the flask. The reaction progress was monitored using TLC analysis. Upon completion of the reaction, confirmed by TLC monitoring, the catalyst was magnetically separated, letting the reaction mixture cool down to room temperature. The final products could be extracted using ethyl acetate. The filtrate was concentrated and further purified via short column chromatography on silica gel using n-hexane/ethyl acetate (9:1) as the eluent. ^{1}H-NMR and ^{13}C-NMR spectra of some products confirmed the structural features of the expected products.

General procedure for the Suzuki–Miyaura reaction

To a round-bottom flask, the following was added, 5 mL of water/ethanol (1:1), aryl halide (1 mmol), phenylboronic acid (1.2 mmol), K_2CO_3 (3 mmol), Fe_3O_4@starch-Co(II) (0.14 mol%). The mixture was heated to 80 °C for a suitable time and kept stirring. Upon completion of the reaction confirmed by TLC, the catalyst nanoparticles were isolated from the reaction mixture. The reaction mixture was cooled down at room temperature, and then, the ethyl acetate was employed to extract the products. The separated organic layer was washed with water and dried with anhydrous $MgSO_4$, then filtered, and finally, after evaporation of the solvent under reduced pressure, the crude product was purified by flash chromatography [n-hexane/ethyl acetate (8:2)] if necessary, to afford the desired purity. The molecular structure of some products was confirmed by GC-FID chromatograph, ^{1}H-NMR, and ^{13}C-NMR spectra and comparing them with those found in the previous papers.

Characterization analysis

The cobalt quantity was measured by AAS analysis. Other analyses, including FT-IR, XRD, FE-SEM, TEM, BET, TGA, EDS, and elemental mapping, were utilized to investigate the details of the catalyst structure and its physicochemical properties.

Results and discussion

Characterization of fabricated catalyst

FT-IR analysis

To determine the chemical structure of the samples, the FT-IR spectra of the bare Fe_3O_4, starch, Fe_3O_4@starch, and Fe_3O_4@starch-Co(II) were recorded (Fig. 1).

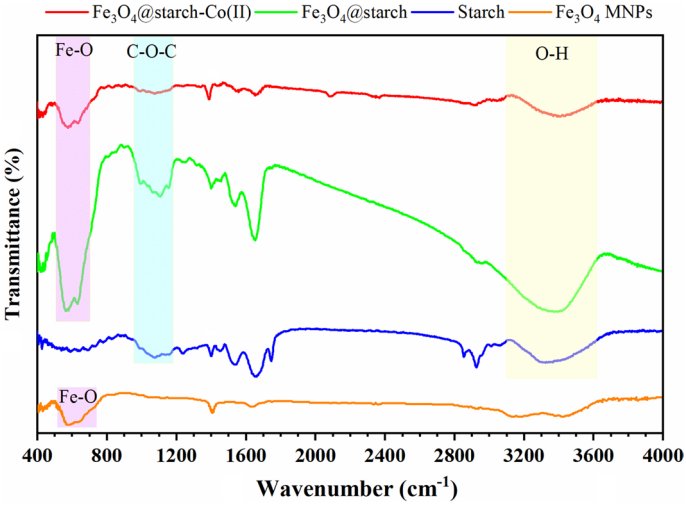

Fig. 1 The FT-IR spectrum of Fe_3O_4, starch, Fe_3O_4@starch, and Fe_3O_4@starch-Co(II)

There are two bands at 557 and 570 cm^{-1} in magnetic samples corresponding to Fe–O bending vibrations [23]. The starch spectrum illustrates some peaks at 1156 cm^{-1}, 1400 cm^{-1}, 1647 cm^{-1}, 2952 cm^{-1}, 3336 cm^{-1}, corresponding to stretching vibration of glycosidic C–O–C, C–O, bending vibration of CH_2, stretching vibration of –CH, stretching vibration of –OH, respectively [1]. In the Fe_3O_4@starch pattern, the characteristic peaks of the magnetic nanoparticles and the starch were integrated, indicating the successful synthesis of the Fe_3O_4@starch structure. In the spectrum of Fe_3O_4@starch-Co(II), the C=O band shifted to a lower wave number (1646 cm^{-1}), and there is an overall decrease in the peak intensity, possibly due to the interaction of the carbonyl functional group with the Co nanoparticles [38]. The overall results from the Fe_3O_4@starch-Co(II) spectrum indicate the successful synthesis of the novel green biocatalyst.

FE-SEM analysis

Scanning electron microscopy is another effective tool to better understand the morphological changes due to the chemical modifications and incorporation of apple seed starch for obtaining Fe_3O_4@starch and Fe_3O_4@starch-Co(II) (Fig. 2). According to Fig. 2, morphological changes happened after coating and immobilization; besides, there was an increase in the size of the nanoparticles after the immobilization of cobalt. These gradual changes confirmed that the final catalyst had been successfully prepared. A similar spherical morphology can be seen in all the images showing the uniform nature of the catalyst nanoparticles. However, in some cases of SEM images of Fe_3O_4@starch-Co(II), there is an aggregation of the particles resulting from the immobilization processes. Also, for the assessment of the average particle size of the fabricated catalyst, a histogram curve was drawn based on 150 particle sizes, and the average particle size was observed at 14.58 nm (Fig. 2e).

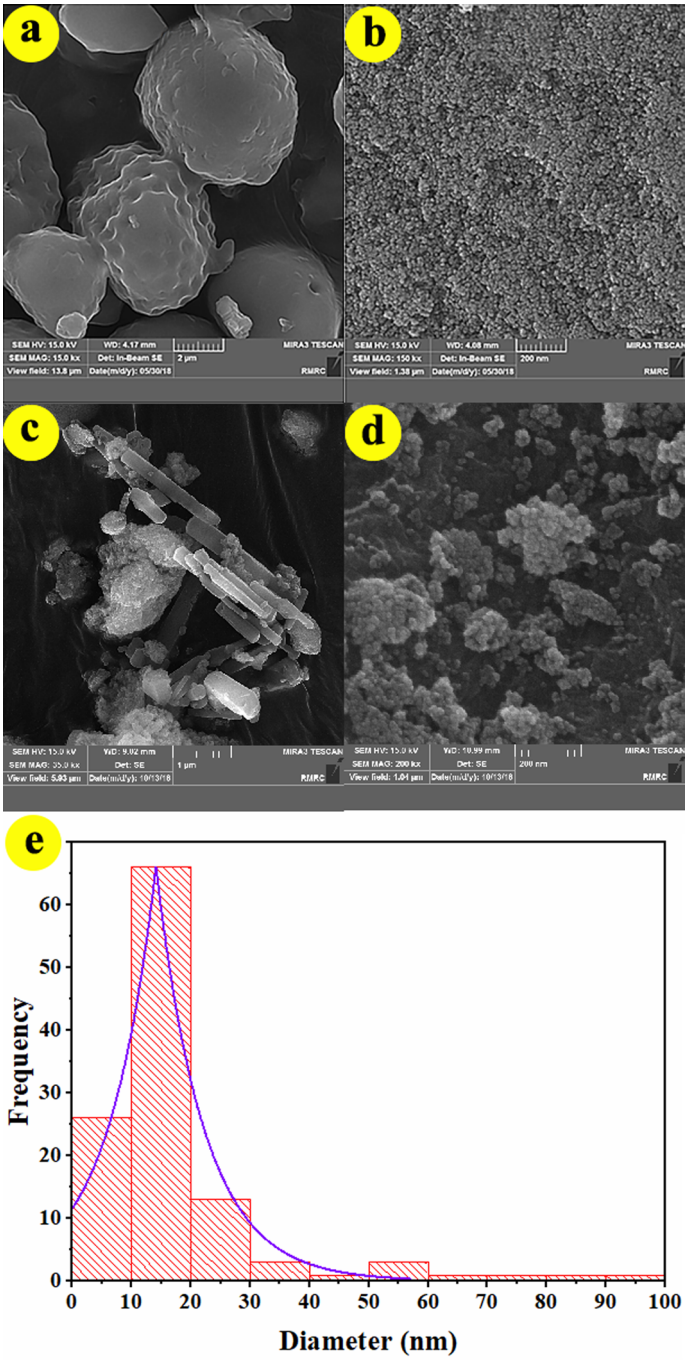

Fig. 2 FE-SEM images of **a** starch, **b** Fe_3O_4@starch, **c**, **d** Fe_3O_4@stach-Co(II), and **e** histogram curve

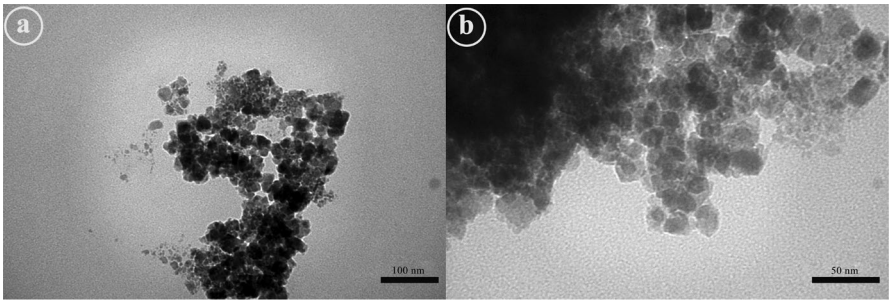

Fig. 3 TEM analysis of Fe_3O_4@Starch-Co(II)

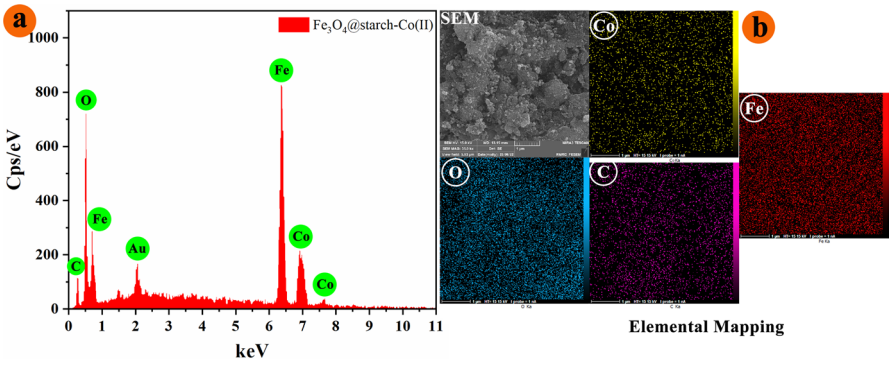

Fig. 4 **a** EDS spectrum and **b** elemental images of Fe_3O_4@starch-Co(II)

TEM analysis

TEM analysis was used to provide more information about the structure of the catalyst. The TEM images of Fe_3O_4@Starch-Co(II) catalyst at different magnifications are shown in Fig. 3. It is evident that the Fe_3O_4 cores (dark segments) were covered with layers of apple seed starch (gray segments).

EDX analysis

EDS spectrum and elemental mapping images presented in Fig. 4a, b corroborated the formation of the green cobalt catalyst. In Fig. 4, the peaks of iron, carbon, and oxygen are observed, indicating the presence of Fe_3O_4 and starch. Further, the EDX spectrum also confirmed the presence of cobalt in the synthesized catalyst. The quantity of anchored cobalt with the bio-support was measured by EDX, and the value was about 8.5%.

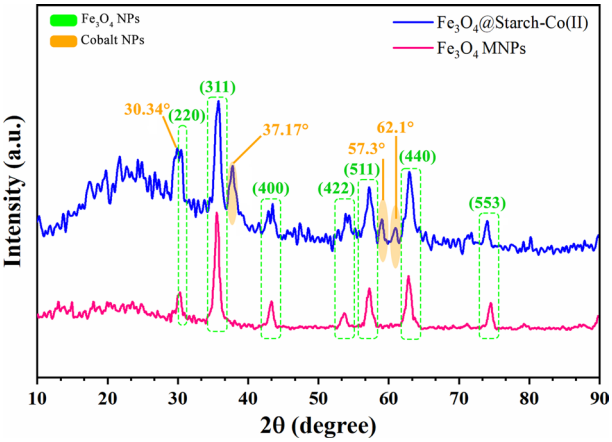

Fig. 5 **a** XRD pattern of Fe_3O_4 MNPs, **b** Fe_3O_4@starch-Co(II)

XRD analysis

X-ray diffraction (XRD) spectrum can provide definitive evidence for the existence of cobalt and iron in our samples (Fig. 5). There are some peaks at 2θ = 30.5°, 35.9°, 43.5°, 53.9°, 57.2°, 63°, and 74.6° existing in both spectra, indicating the inverse cubic spinel structure of Fe_3O_4 (JCPDS 85-1436) [1, 23]. The XRD pattern of Fe_3O_4@starch-Co(II) shows that there is a decrease in the intensity of the Fe_3O_4 peaks because of chemical modifications; however, the phase of the magnetite nanoparticles has not been changed. Also, the peaks at 2θ = 30.34°, 37.17°, 57.3°, and 62.1° are related to the cubic phase of the crystalline structure of the cobalt nanoparticles [39, 40].

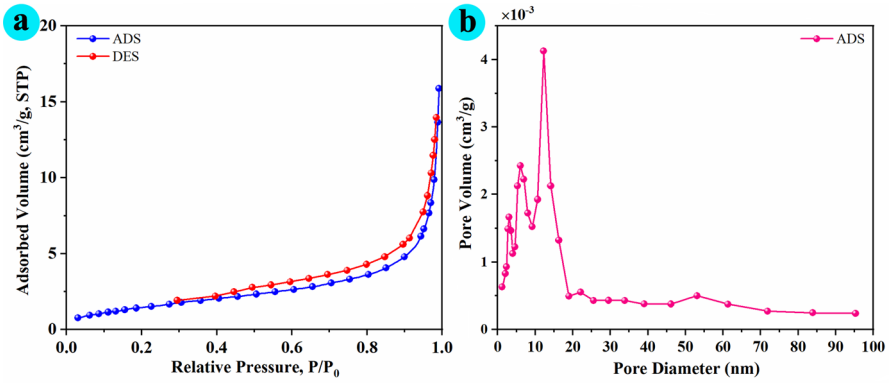

Fig. 6 **a** The N_2 adsorption–desorption isotherm and **b** BJH curve of the Fe_3O_4@starch-Co(II)

BET analysis

The textural properties of the synthesized catalyst, including surface area, pore size, and pore volume, were studied using BET and BJH analyses. These analyses were conducted at 77 K utilizing N_2 adsorption, and the related diagrams are shown in Fig. 6a. Based on IUPAC classification, this mesoporous catalyst has a type IV isotherm with H4-type hysteresis loops. According to the obtained data from these analyses, the BET surface area ($a_{s,BET}$) of Fe_3O_4@starch-Co(II) catalyst is 18.92 m^2/g, and the pore volume is 7.62 cm^3/g, and the mean pore diameter of this mesoporous material is 12.68 nm. The hysteresis loop, which is an indication for mesoporous structures, appears in adsorption–desorption measurements, and the fabricated catalyst is mesopore based on the average diameter information and hysteresis loop. Furthermore, the most frequent radius pore in the Fe_3O_4@starch-Co(II) catalyst is 13.06 nm, as per the BJH curve (Fig. 6b).

TGA analysis

The results of the TGA analyses of starch, Fe_3O_4@starch, and Fe_3O_4@starch-Co(II) are displayed in Fig. 7. Fe_3O_4@starch and Fe_3O_4@starch-Co(II) thermograms show two stages of thermal weight loss, and the first stage (under 200 °C) is attributed to the escape of water molecules. The second stage of weight loss started from 225 to 570 °C, corresponding to the thermal decomposition of starch saccharides ring degradation. Based on the bare starch thermogram, the resulting weight loss is about 87.39%. When starch combines with the Fe_3O_4 MNPs, the weight loss is slower than bare starch, and about 26.22% and the weight loss in Fe_3O_4@starch-Co(II) is about

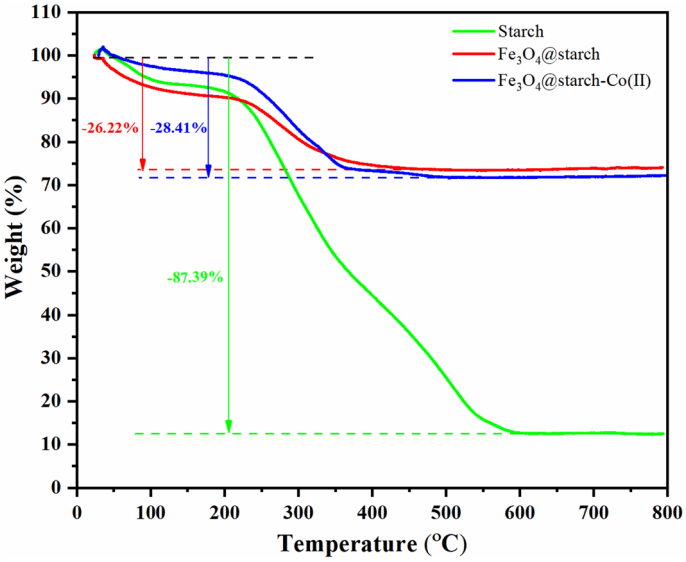

Fig. 7 TGA curve of starch, Fe_3O_4@starch, and Fe_3O_4@starch-Co(II)

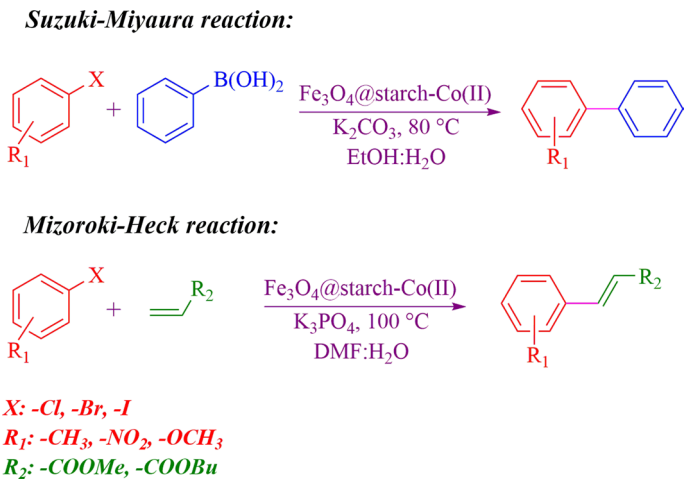

Scheme 2 Suzuki–Miyaura and Mizoroki–Heck cross-coupling reactions catalyzed by Fe_3O_4@starch-Co(II)

28.41%. This subject reveals that the starch was successfully incorporated in Fe_3O_4 MNPs.

Atomic absorption spectroscopy (AAs) analysis

Finally, to exactly determine the quantity of the loaded cobalt in the catalyst, atomic absorption spectroscopy was performed. From the AAS results, it was calculated a loading at 1.4 mmol/g of cobalt in the catalyst, which is well consistent with the EDX result.

Catalytic activity

Assessing the performance of our green nanocatalyst, we were interested in utilizing it in C–C bond formation *via* Suzuki–Miyaura and Mizoroki–Heck cross-coupling reactions (Scheme 2).

Suzuki–Miyaura coupling reaction

Optimization of reaction Before assessing the catalytic performance, optimization of the reaction terms was conducted to maximize the reaction efficiency. Parameters including temperature, solvent, base system, and the amount of the catalyst are optimized. Hence, the reaction of phenylboronic acid (1.2 mmol) with iodobenzene (1.0 mmol) was selected as a model reaction to determine the optimized conditions. Different amounts of the catalyst were employed to determine the optimum value. According to Table 1, as the catalyst amount increased gradually, the reaction efficiency was enhanced because of the availability of more catalytic sites (Table 1, entries 1–5). As shown in Table 1, 0.14 mol% is the optimum value to

Table 1 Optimization of the reaction conditions for the Suzuki–Miyaura cross-coupling reaction[a]

Entry	Catalyst amount (% mol)	Base	Solvent	Temperature (°C)	Time (min)	Yield (%)
1	–	K_2CO_3	H_2O	100	24	–
2	0.035	K_2CO_3	H_2O	100	55	65
3	0.07	K_2CO_3	H_2O	100	55	70
4	0.14	K_2CO_3	H_2O	100	45	85
5	0.21	K_2CO_3	H_2O	100	45	84
6	0.001(g)[a]	K_2CO_3	H_2O	100	24	15
7	0.001(g)[b]	K_2CO_3	H_2O	100	24	Trace
8	0.14[c]	K_2CO_3	H_2O	100	24	35
9	0.14	Na_2CO_3	H_2O	100	60	85
10	0.14	KOH	H_2O	100	50	55
11	0.14	NaOH	H_2O	100	50	50
12	0.14	K_3PO_4	H_2O	100	45	80
13	0.14	Et_3N	H_2O	100	55	80
14	0.14	K_2CO_3	EtOH	100	45	80
15	0.14	K_2CO_3	H_2O/EtOH (1/1)	100	45	93
16	0.14	K_2CO_3	CH_3COOEt	100	50	65
17	0.14	K_2CO_3	DMF	100	50	75
18	**0.14**	**K_2CO_3**	**H_2O/EtOH (1/1)**	**80**	**45**	**90**
19	0.14	K_2CO_3	H_2O/EtOH (1/1)	60	55	75
20	0.14	K_2CO_3	H_2O/EtOH (1/1)	R.T	6	-

[a]Reaction in the presence of Fe_3O_4NPs

[b]Reaction in the presence of Fe_3O_4@starch

[c]Reaction in the presence of $Co(OAc)_2.4H_2O$

The bold entries in Tables 1 are related to optimal conditions for the Suzuki-Miyaura and Mizoroki-Heck cross-coupling model reactions

achieve a satisfactory efficiency. Also, the reaction was performed in the presence of Fe_3O_4 NPs, Fe_3O_4@starch, and $Co(OAc)_2{\cdot}4H_2O$, which did not produce satisfactory results (Table 1, entries 6–8). The Suzuki–Miyaura coupling reaction proceeds in the presence of a base; hence, finding the most effective type of base for this reaction is crucial. The model reaction was carried out in the presence of different bases. According to Table 1, entries 4, 9–13, it was found that K_2CO_3 provided the best result. Solvents play a pivotal role in controlling the reaction both thermodynamically and kinetically. Therefore, selecting a proper solvent for this reaction is important to maximize the reaction efficiency. The model reaction was conducted

in the presence of different solvents, and according to Table 1, entries 4, 14–17, it was found that a mixture of EtOH and H_2O with a 1:1 molar ratio afforded the highest efficiency within a shorter time. Another important reaction term is temperature, so its influence on the reaction conditions is outlined in Table 1, entries 15, 18–20. Considering the reaction yields and times, 80 °C was selected as the best value for this reaction.

Scope of reaction To assess the performance of this novel green catalyst and understand the generality of its application in the Suzuki–Miyaura reaction, different types of aryl halides (aryl chlorides, aryl bromides, and aryl iodides) reacted with phenylboronic acid. The results are presented in Table 2. The ability of halogens as a leaving group is ordered as the following: I > Br > Cl; thus, the results of Table 2 are consistent with our expectations. Firstly, the reaction proceeds faster with aryl iodides than aryl bromide and aryl chloride, and aryl chloride needs much time with lower efficiency. Further, Turnover numbers (TON) and turnover frequency (TOF) are listed for all products in Table 2.

Table 2 Suzuki–Miyaura coupling reactions of aryl halides with $PhB(OH)_2$[a]

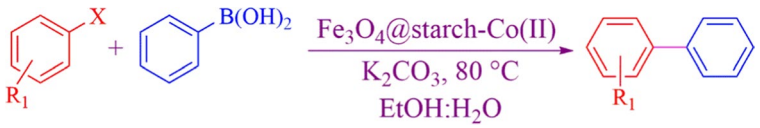

Entry	Aryl halide	Product	Time (min)	Yield (%)	TON [b]	TOF [c]
1	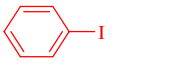	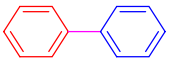	45	90	642	856
2	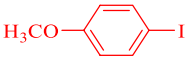	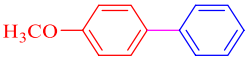	45	80	571	761
3	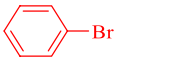	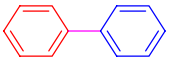	60	85	607	607
4	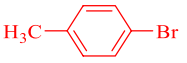	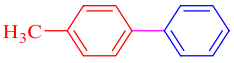	75	80	571	456
5	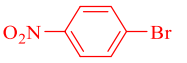	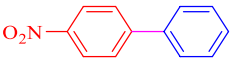	45	85	607	809
6	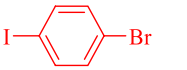	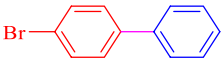	50	87	621	745
7	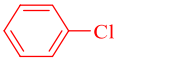	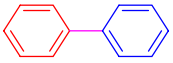	240	50	357	89

[a]Reaction conditions: Phenyl boronic acid (1.2 mmol), aryl halide (1.0 mmol), K_2CO_3 (3 mmol), EtOH/H_2O (1:1) (5 mL) and catalyst (0.14% mol) at 80 °C

[b]TON: Turnover number, product yield per mol of Co(II)

[c]TOF: Turnover frequency, TON/reaction time (h)

Mizoroki–Heck coupling reaction

Optimization of reaction With good results from utilizing this new catalyst in the Suzuki–Miyaura reaction, we were motivated to evaluate its performance in the Mizoroki–Heck reaction. Firstly, we need to find the optimized reaction conditions as we had before. The reaction between iodobenzene (1 mmol) and methyl acrylate (1.5 mmol) was considered as a model reaction to optimize the reaction terms, including temperature, catalyst quantity, type of the solvent, and base. To determine the optimum catalyst

Table 3 Optimization of the reaction conditions for the Mizoroki–Heck reaction [a]

Entry	Catalyst amount (% mol)	Base	Solvent	Temperature (°C)	Time (min)	Yield (%)
1	–	K_2CO_3	H_2O	100	24	–
2	0.14	K_2CO_3	H_2O	100	80	55
3	0.28	K_2CO_3	H_2O	100	70	68
4	0.42	K_2CO_3	H_2O	100	65	70
5	0.56	K_2CO_3	H_2O	100	65	72
6	0.004 (g)[a]	K_2CO_3	H_2O	100	24	10
7	0.004 (g)[b]	K_2CO_3	H_2O	100	24	Trace
8	0.42[c]	K_2CO_3	H_2O	100	24	30
9	0.42	Na_2CO_3	H_2O	100	65	65
10	0.42	KOH	H_2O	100	65	70
11	0.42	NaOH	H_2O	100	70	60
12	0.42	K_3PO_4	H_2O	100	60	75
13	0.42	Et_3N	H_2O	100	60	70
14	0.42	K_3PO_4	EtOH	100	70	65
15	0.42	K_3PO_4	DMF	100	60	80
16	0.42	K_3PO_4	DMSO	100	80	50
17	0.42	K_3PO_4	PEG	100	80	45
18	**0.42**	**K_3PO_4**	**H_2O/DMF (1/1)**	**100**	**55**	**85**
19	0.42	K_3PO_4	H_2O/DMF (1/1)	120	55	87
20	0.42	K_3PO_4	H_2O/DMF (1/1)	80	65	70
21	0.42	K_3PO_4	H_2O/DMF (1/1)	R.T	6	–

[a]Reaction in the presence of Fe_3O_4 NPs

[b]Reaction in the presence of Fe_3O_4@starch

[c]Reaction in the presence of $Co(OAc)_2{\cdot}4H_2O$

The bold entries in 3 are related to optimal conditions for the Suzuki-Miyaura and Mizoroki-Heck cross-coupling model reactions

quantity, the model reaction was performed in the presence of different amounts of the catalyst (Table 3, entries 1–5). On the other side, to clearly understand the exact role of the catalyst in this reaction, the reaction was carried out in the absence of the catalyst and then in the presence of Fe_3O_4 NPs, Fe_3O_4@starch and $Co(OAc)_2{\cdot}4H_2O$, respectively (Table 3, entries 6–8). Finally, it was found that 0.42 mol% of the catalyst is the optimum value in this reaction. Considering the crucial role of the base in preventing the formation of homo-coupling products and neutralizing hydrogen halides [41], finding a suitable base for this reaction is important. Hence, the reaction was carried out in the presence of different bases, and it was found that K_3PO_4 is the most suitable base for this reaction (Table 3, entries 4, 9–13). The reaction was carried out in the presence of different solvents and solvent mixtures. From Table 3, entries 12, 14–18, a mixture of DMF and H_2O in a 1:1 ratio as solvent provided the best result. Again, the reaction was conducted at various temperatures, and our investigations showed the optimal temperature is 100 °C for this reaction (Table 3, entries 18–21). The optimal temperature is 100 °C for this reaction (Table 3, entries 18–21).

Scope of reaction A wide variety of aryl halides reacted with different olefins under the optimized conditions to assess the catalytic performance of this new nano-biocatalyst in the Mizoroki–Heck reaction. The oxidative addition, which is the insertion of Co into the carbon halide bond, is the first step, and it is expected the reaction with aryl iodide will be faster than aryl bromide and aryl chloride because of the weaker covalent bond. According to Table 4, our expectation is consistent with the reaction results. The reaction with aryl chloride took a long time with low efficiency, but it is desirable as there are many reported cobalt catalytic systems showing no activity with aryl chloride substrates in the Mizoroki–Heck reaction [42, 43]. The highly active nature of this nano-biocatalyst possibly is the result of good synergistic effects of cobalt nanoparticles with ligands anchoring on Fe_3O_4 nanoparticles and good dispersion of cobalt nanoparticles. The values of TON and TOF for all products are shown in Table 4.

Mechanism of reaction

The probable mechanism of the Mizoroki–Heck coupling reaction was presented in Scheme 3. We believe that when the Fe_3O_4@starch-Co(II) catalyst is exposed to a substituted aryl halide, the oxidation state of Co(II) transforms to Co(IV), and the precursor A is formed in the oxidative addition stage. In the complexation stage, the alkyl methacrylate is reacted with species A to produce the intermediate B, which then undergoes deprotonation to form species C in the presence of the base (K_3PO_4). Finally, through reductive elimination and regeneration of the catalyst's starting state, the desired product is produced from the C species.

Catalytic activity comparison

For evaluating the performance of the newly prepared nano-biocatalyst in the coupling reaction of methyl acrylate with iodobenzene, the obtained results were

Table 4 Mizoroki–Heck coupling reactions of aryl halides with olefins [a]

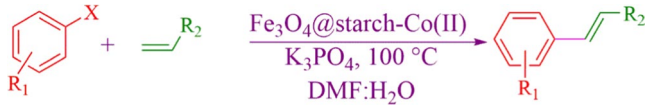

Entry	Aryl halide	Olefin	Product	Time (min)	Yield (%)	TON [b]	TOF [c]
1	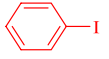		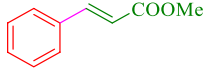	55	85	202	221
2	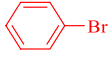		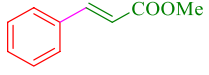	90	78	185	123
3	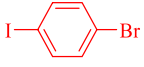		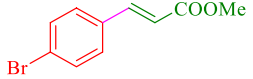	55	80	190	208
4	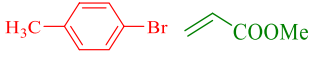		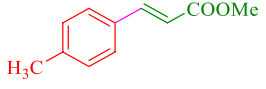	110	75	178	98
5	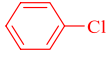	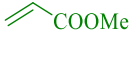	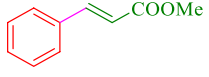	300	30	71	14
6	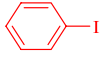	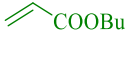	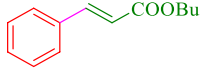	55	82	195	214
7	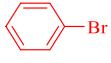	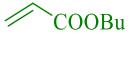	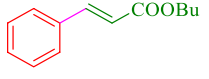	85	75	178	127

Table 4 (continued)

[a]Reaction conditions: aryl halide (1.0 mmol), olefin (1.5 mmol), K_3PO_4 (4.0 mmol), catalyst (0.42% mol), DMF/H_2O (1:1) (3 mL), at 100 °C

[b]TON: turnover number, product yield/per mol of Co(II)

[c]TOF: turnover frequency, TON/time of reaction (h)

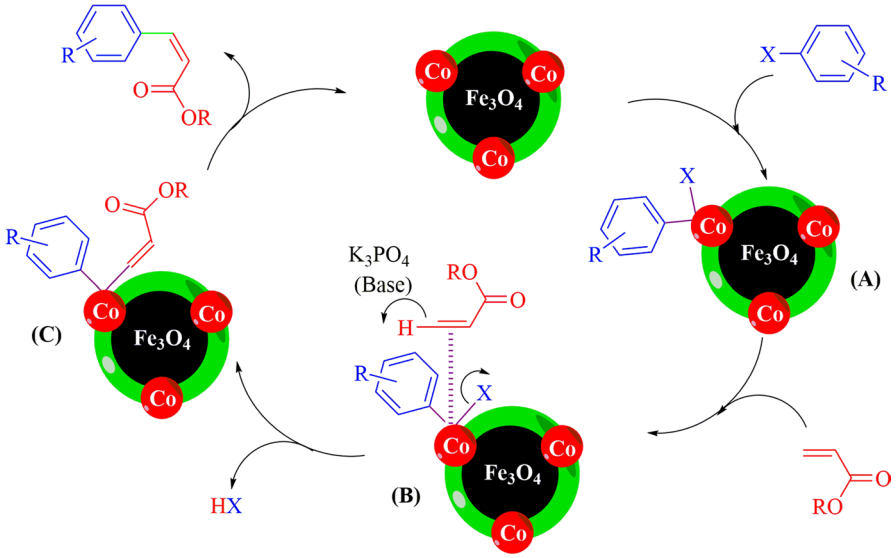

Scheme 3 Proposed mechanism for the Mizoroki–Heck coupling reaction in the presence of Fe_3O_4@starch-Co(II)

compared with some of the published heterogeneous catalysts (Table 5). Some obvious advantages that our catalyst has over other supported catalytic systems are easy magnetic separation, low preparation cost, high efficiency, shorter reaction time, lower temperature, greener media, minimizing metal contamination, high recyclability, elimination of additional equipment like a microwave oven and using a tiny amount of the catalyst.

Catalyst reusability

Catalyst recyclability plays a pivotal role in industrial applications as it is preferable to be highly active after separation and recycling in order to save time and money [1]. Therefore, the catalyst recycling was evaluated by performing the Suzuki–Miyaura reaction of iodobenzene with phenylboronic acid (Model reaction) at the optimized conditions. After completion of the reaction, the catalyst was magnetically isolated and washed thoroughly with ethanol and distilled water, followed by drying in an oven at 60 °C. According to Fig. 8, the reused catalyst could be employed for four runs without significant loss in its activity. The FE-SEM images of the fresh and reused catalysts are presented in Fig. 9, and it was found that there was no change in the nature and morphology of the catalyst particles. Also, EDX analysis presented in Fig. 10 proves cobalt-leaching was negligible, and the composition of the catalyst was roughly stable even after four consecutive runs.

Leaching is a process deteriorating the catalyst performance; in fact, the metal ions are gradually detached from the support, and the catalyst performance will be diminished [23]. Thus, the reaction between iodobenzene and phenylboronic acid

Table 5 Comparing Fe_3O_4@starch-Co(II) results with previous literature in the Mizoroki–Heck reaction[a]

Entry	Catalyst	Solvent	Temperature (°C)	Time (h:min)	Yield (%)	References
1	Co–NHC@MWCNTs	PEG	80	05:00	85	[46]
2	SiO_2-Fe(II)	PEG	130	01:30	85	[47]
3	Co@MNPs/CS	PEG	80	01:00	53	[39]
4	Nano Co	NMP	140	16:00	85	[48]
5	Co hollow nanospheres	NMP	130	16:00	73	[49]
6	Co/Al_2O_3	NMP	150	24:00	56	[50]
7	Co-B	Water/DMF (5:5)	130	12:00	98	[43]
8	Co-IL@MWCNTs	Toluene	100	03:00	87	[42]
9	Ni(II)–DABCO@SiO_2	DMF	100	03:00	97	[51]
10	Nano Co	NMP	120	08:00	90	[52]
11	Fe_3O_4@TEA-Pd(II)	DMF	80	00:14	96	[23]
12	Co-MS@MNPs/CS	PEG	80	01:00	88	[39]
13	MNP@Seed starch@FR-Co	Water/DMF (1:1)	100	00:55	92	[16]
14	MNP@PAMAM-Co	Water/DMF (1:1)	100	00:50	90	[44]
15	Fe_3O_4@starch-Co(II)	Water/DMF (1:1)	100	00:55	85	This work

MWCNT multi-walled carbon nanotubes, *MNPs* magnetic nanoparticles, *IL* ionic liquid, *DABCO* 1,4-diazobicyclo[2.2.2]octane, *TEA* triethanolamine

was carried out under optimal conditions in order to understand the content of metal ions detached from the surface at half of the reaction time. The catalyst particles were isolated from the reaction medium using a magnet and then allowed the reaction to go forward for 2 h without the catalyst. The reaction was monitored using the TLC technique. TLC analyses showed that no further progress in coupling reaction was made, indicating that there was no tangible leaching phenomenon.

In order to determine the nature of the catalyst, we carried out a hot filtration test based on previous studies [53, 54]. The purpose of this test was to determine whether or not the Fe_3O_4@starch-Co(II) catalyst operates in a heterogeneous nature. Both the Mizoroki–Heck and Suzuki–Miyaura reactions were carried out for 1 h in the presence of a Fe_3O_4@starch-Co(II) catalyst, which was then recovered from the reaction media using a magnet. After that, the filtrate was allowed to react for another 1 h under the same conditions to complete the reaction time. The Mizoroki–Heck and

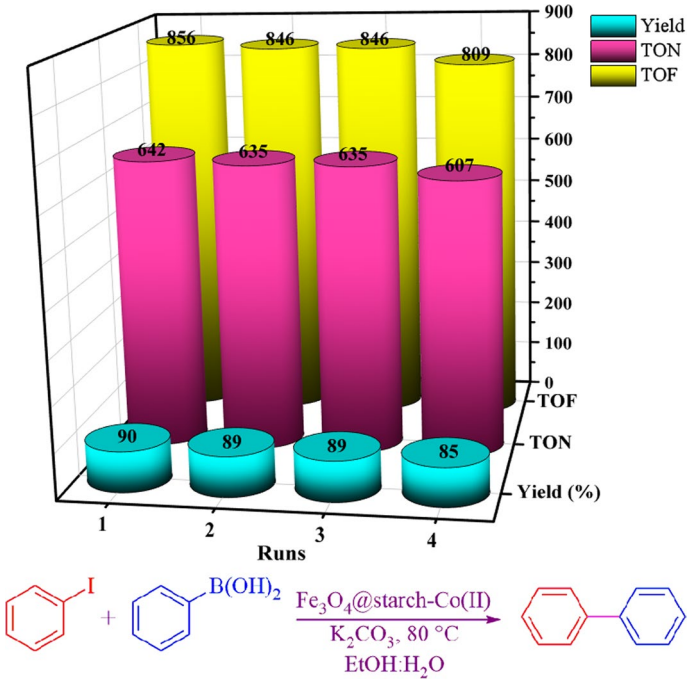

Fig. 8 Recyclability in the Suzuki–Miyaura reaction

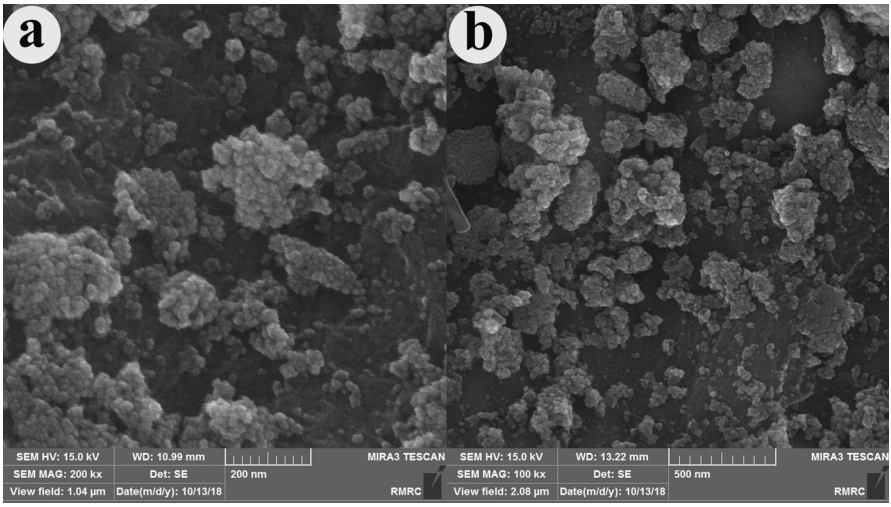

Fig. 9 FE-SEM images of **a** fresh catalyst and **b** reused catalyst after four runs in the Suzuki–Miyaura reaction

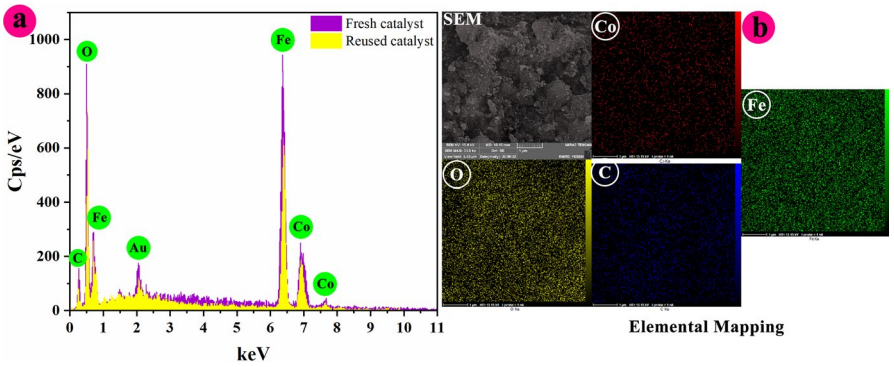

Fig. 10 **a** EDS spectrum of fresh catalyst and reused catalyst and **b** elemental images of reused catalyst after four runs in the Suzuki–Miyaura reaction

Suzuki–Miyaura reactions did not advance with the filtrate, indicating that Fe_3O_4@starch-Co(II) possessed a heterogeneous nature.

The results proved the heterogeneous nature of our new catalyst, and this would be a reasonable conclusion that cobalt is strongly attached to the surface of the Fe_3O_4@starch structure.

Conclusion

In summary, we are very pleased to disclose a report on the application of starch derivated apple seed as a green and sustainable catalyst support in Suzuki–Miyaura and Mizoroki–Heck reactions. Fe_3O_4@starch showed its potential as a suitable host for cobalt nanoparticles. Fe_3O_4@starch-Co(II) catalyst offers advantages including high efficiency, low cost, high chemical stability, low toxicity, and magnetic separation. The Fe_3O_4@starch-Co(II) catalyst was employed in Mizoroki–Heck and Suzuki–Miyaura reactions, and it showed high reactivity and selectivity in those reactions. In comparison with other previous literature on cobalt-catalyzed cross-coupling reactions, it minimized time and energy consumption. Ultimately, Fe_3O_4@starch-Co(II) reusability examination proved negligible cobalt leaching during the reaction, and it could be utilized for four consecutive runs without significant loss in the activity.

Supplementary Information The online version contains supplementary material available at https://doi.org/10.1007/s11164-022-04818-2.

Acknowledgements The authors sincerely acknowledge the Research Council of Semnan University for supporting this work.

Availability of data and materials My manuscript has data included as electronic supplementary material.

Code availability Not applicable.

Declarations

Conflict of interests All authors are aware of the submission and agree to its publication, and have no conflicts of interest.

References

1. A. Marandi, E. Nasiri, N. Koukabi, F. Seidi, Int. J. Biol. Macromol. **190**, 61 (2021)
2. D. Khorsandi, A. Zarepour, I. Rezazadeh, M. Ghomi, R. Ghanbari, A. Zarrabi, F. T. Esfahani, N. Mojahed, M. Baghayeri, E. N. Zare, P. Makvandi (2022) Ionic liquid-based materials for electrochemical biosensing. Clin. Transl. Discov. **2**, e127 (2022).
3. R. Ghanbari, D. Khorsandi, A. Zarepour, M. Ghomi, A. Fahimipour, Z. Tavakkoliamol, and A. Zarrabi, Mater. Chem. Horizons (2022).
4. H. Mahdavi and R. Ghanbari, J. Ind. Eng. Chem. **113,** 132 (2022).
5. T. Baran, N. Yılmaz Baran, A. Menteş, Appl. Organomet. Chem. **32**, 4076 (2018)
6. S.M.S. Arabi, J. Alicata, D. Hanigan, S.R. Hiibel, Int. J. Greenh. Gas Control **111**, 103472 (2021)
7. B. Rajarathinam, K. Kumaravel, G. Vasuki, RSC Adv. **6**, 73848 (2016)
8. A. Marandi, N. Koukabi, M.A. Zolfigol, Res. Chem. Intermed. **47**, 3145 (2021)
9. A. Marandi, E. Kolvari, M. Gilandoust, M.A. Zolfigol, Diam. Relat. Mater. **124**, 108908 (2022)
10. P. Verma, S. Pal, S. Chauhan, A. Mishra, I. Sinha, S. Singh, V. Srivastava, J. Mol. Struct. **1203**, 127410 (2020)
11. S. Sabaqian, F. Nemati, H.T. Nahzomi, M.M. Heravi, Carbohydr. Polym. **177**, 165 (2017)
12. N. Shafiei, M. Nasrollahzadeh, T. Baran, N.Y. Baran, M. Shokouhimehr, Carbohydr. Polym. **262**, 117920 (2021)
13. S. Zolfagharinia, N. Koukabi, E. Kolvari, RSC Adv. **6**, 113844 (2016)
14. E. Kolvari, S. Zolfagharinia, RSC Adv. **6**, 93963 (2016)
15. M.A. Khalilzadeh, S.Y. Kim, H.W. Jang, R. Luque, R.S. Varma, R.A. Venditti, M. Shokouhimehr, Mater. Today Chem. **24**, 100869 (2022)
16. M. Arghan, N. Koukabi, E. Kolvari, Appl. Organomet. Chem. **33**, e5075 (2019)
17. D. Yang, L. Yu, H. Chen, Y. Yu, Y. Xu, J. Sun, Y. Wang, Polym. Bull. **74**, 5231 (2017)
18. A. Min Tong, W. Ya Lu, J. He Xu, G. Qiang Lin, Bioorg. Med. Chem. Lett. **14**, 2095 (2004)
19. M. Manzoor, J. Singh, A. Gani, LWT **151**, 112138 (2021)
20. T. Baran, J. Colloid Interface Sci. **496**, 446 (2017)
21. A. Shaabani, A. Rahmati, Z. Badri, Catal. Commun. **9**, 13 (2008)
22. H. Elkhenany, M. Abd Elkodous, N.I. Ghoneim, T.A. Ahmed, S.M. Ahmed, I.K. Mohamed, N. El-Badri, Int. J. Biol. Macromol. **143**, 763 (2020)
23. A. Marandi, N. Koukabi, Colloids Surfaces A Physicochem. Eng. Asp. **621**, 126597 (2021)
24. F. Chen, M. Huang, Y. Li, Ind. Eng. Chem. Res. **53**, 8339 (2014)
25. T. Baran, A. Menteş, J. Organomet. Chem. **803**, 30 (2016)
26. H.D. Güzel, M. Çalışkan, T. Baran, J. Phys. Chem. Solids **167**, 110777 (2022)
27. K. Hong, M. Sajjadi, J.M. Suh, K. Zhang, M. Nasrollahzadeh, H.W. Jang, R.S. Varma, M. Shokouhimehr, A.C.S. Appl, Nano Mater. **3**, 2070 (2020)
28. N. Khadir, G. Tavakoli, A. Assoud, M. Bagherzadeh, D.M. Boghaei, Inorganica Chim. Acta **440**, 107 (2016)
29. T. Baran, I. Sargin, M. Kaya, A. Menteş, J. Mol. Catal. A Chem. **420**, 216 (2016)
30. M. Nasrollahzadeh, R. Bakhshali-Dehkordi, T.A. Kamali, Y. Orooji, M. Shokouhimehr, J. Mol. Struct. **1244**, 130873 (2021)
31. K.-H. Choi, M. Shokouhimehr, Y.-E. Sung, Bull. Korean Chem. Soc. **34**, 1477 (2013)
32. Y. Wang, C. Lu, G. Yang, Z. Chen, J. Nie, React. Funct. Polym. **110**, 38 (2017)
33. T. Baran, Int. J. Biol. Macromol. **127**, 232 (2019)
34. A. Ahadi, S. Rostamnia, P. Panahi, L.D. Wilson, Q. Kong, Z. An, M. Shokouhimehr, Catal. **9**, 140 (2019)
35. T. Baran, A. Menteş, J. Mol. Struct. **1122**, 111 (2016)

36. T. Baran, İ Sargın, M. Kaya, P. Mulerčikas, S. Kazlauskaitė, A. Menteş, Chem. Eng. J. **331**, 102 (2018)
37. M. Shokouhimehr, J.-H. Kim, Y.-S. Lee, Synlett **2006**, 0618 (2006)
38. R.J. Kalbasi, F. Zamani, RSC Adv. **4**, 7444 (2014)
39. A.R. Hajipour, F. Rezaei, Z. Khorsandi, Green Chem. **19**, 1353 (2017)
40. A.R. Hajipour, Z. Khorsandi, Appl. Organomet. Chem. **34**, e5398 (2020)
41. M. Arghan, N. Koukabi, E. Kolvari, Appl. Organomet. Chem. **32**, e4346 (2018)
42. A.R. Hajipour, Z. Khorsandi, H. Karimi, Appl. Organomet. Chem. **29**, 805 (2015)
43. Z. Zhu, J. Ma, L. Xu, L. Xu, H. Li, H. Li, ACS Catal. **2**, 2119 (2012)
44. M. Arghan, N. Koukabi, E. Kolvari, Appl. Organomet. Chem. **33**, e4823 (2019)
45. W. Affo, H. Ohmiya, T. Fujioka, Y. Ikeda, T. Nakamura, H. Yorimitsu, K. Oshima, Y. Imamura, T. Mizuta, K. Miyoshi, J. Am. Chem. Soc. **128**, 8068 (2006)
46. A.R. Hajipour, Z. Khorsandi, Catal. Commun. **77**, 1 (2016)
47. A.R. Hajipour, G. Azizi, Green Chem. **15**, 1030 (2013)
48. H. Qi, W. Zhang, X. Wang, H. Li, J. Chen, K. Peng, M. Shao, Catal. Commun. **10**, 1178 (2009)
49. P. Zhou, Y. Li, P. Sun, J. Zhou, and J. Bao, Chem. Commun. **43,** 1418 (2007).
50. S. Iyer, V.V. Thakur, J. Mol. Catal. A Chem. **157**, 275 (2000)
51. A.R. Hajipour, P. Abolfathi, Catal. Letters **147**, 188 (2017)
52. K.S. Jithendra Kumara, G. Krishnamurthy, B.E. Kumara Swamy, N. Sunil-Kumar, M. Kumar, J. Porous Mater. **24**, 1095 (2017)
53. M. Çalışkan, T. Baran, Appl. Clay Sci. **219**, 106433 (2022)
54. M. Çalışkan, T. Baran, M. Nasrollahzadeh, J. Phys. Chem. Solids **152**, 109968 (2021)